Journal of Energy Storage 62 (2023) 106839

Contents lists available at ScienceDirect

Journal of Energy Storage

journal homepage: www.elsevier.com/locate/est

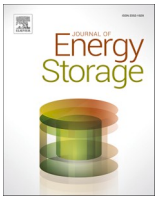

Research papers

Degradation analysis of 18650 cylindrical cell battery pack with immersion liquid cooling system. Part 1: Aging assessment at pack level

D. Koster [c,d], A. Marongiu [a,*], D. Chahardahcherik [b], C.F. Braun [b], D. Schulte [a,b], E. Figgemeier [c,d,e]

[a] BatterieIngenieure South Europe SL., Derio, Spain
[b] BatterieIngenieure GmbH, Aachen, Germany
[c] Juelich Aachen Research Alliance, JARA-Energy, Germany
[d] Forschungszentrum Juelich GmbH, IEK-12, Helmholtz-Institut Münster, co ISEA of RWTH Aachen University, 52066 Aachen, Germany
[e] Aging Processes and Lifetime Prediction of Batteries, Institute for Power Electronics and Electrical Drives (ISEA), RWTH Aachen University, 52066 Aachen, Germany

ARTICLE INFO

Keywords:
lithium-ion batteries
Thermal management
Immersed cooling
Inhomogeneous degradation

ABSTRACT

Temperature is a fundamental factor when designing battery packs, therefore thermal management is essential to guarantee performance, safety, and lifetime in the application. In the first of a series of two papers, this work presents an experimental study of degradation of two identical 18650-battery packs with two different cooling systems, one with air cooling and one with a novel immersed cooling system. By means of cycling tests, the behavior of the two packs subjected to same degradation profiles but different cell temperature distribution is quantitatively and qualitatively analyzed. The results show that homogeneous temperature distribution can be kept up to a maximum temperature difference of 1.5 °C between the cells contained in the immersed-cooled pack against 15 °C between the cells included in the air-cooled pack. This generates an increase of capacity retention up to 3.3 % for the immersed-cooled pack after 600 cycles. Even though temperature is kept uniform, immersed cooled pack experienced cell failures, which were not presented in the air-cooled pack. Application-oriented analysis discusses possible merits and drawbacks of implementing such solution in the application, highlighting that in some cases a reduction up to 25 % of pack specific energy can be experienced when implementing immersed-cooling system.

1. Introduction

Electrochemical energy storage systems (ESS) play a key role in the electrification and hence de-carbonization of our society. Among the different ESS available on the market, Li-ion batteries still represent the leading technology as they exhibit outstanding properties, such as high energy efficiency, low self-discharge rate, lack of memory effect, high cycle life and high energy and power density [1]. These advantages make them the first choice for powering battery electric vehicles (BEVs), where stringent requirements must be fulfilled to reach the desired driving ranges and charging rates [2]. However, due to the presence of different degradation processes during operation and even during storage, Li-ion cells suffer from a continuous loss of performance, which in BEVs can be translated in loss of energy i.e., capacity fade. This effect drastically reduces the driving range of battery powered vehicles, where the available energy densities are no longer sufficient as soon as the battery state-of-health (SoH) falls below 80 % [3]. Consequently, one of the major challenges in BEVs is to improve energy management strategies to slow down degradation processes and thus extend the lifetime of the ESS, which would eventually result in an enhanced CO_2 balance sheet and customer benefits [2].

Temperature is a critical parameter that considerably influences the aging behavior of a Li-ion battery [4]. It is generally and commonly ascertained that the optimum operating temperature of Li-ion cells lies in a range within 15 °C and 35 °C [5]. At lower temperatures, performance degradation is observed, which may be attributed to a limitation in solid state diffusion as well as to a decrease in electrolyte conductivity [6]. Moreover, with decreasing temperature the intercalation reaction kinetics become more and more difficult, which can be attributed to an increase of charge transfer resistance at both anode and cathode [7,8].

* Corresponding author: BatterieIngenieure South Europe SL., Astondo Bidea (BIC Bizkaia – Building 612), CP: 48160 Derio, Spain.
E-mail address: info@batt-ing.de (A. Marongiu).
URL: https://batteryengineers.com (A. Marongiu).

https://doi.org/10.1016/j.est.2023.106839
Received 2 September 2022; Received in revised form 27 December 2022; Accepted 4 February 2023
Available online 28 February 2023

At temperatures above 35 °C aging processes are highly accelerated, resulting in energy (capacity) and power losses, which negatively impact battery lifetime. Aging processes occurring at elevated temperatures are diverse and can be related to exothermic reactions during the charging and discharging process, such as the decomposition of the conducting salt in the electrolyte, phase changes of the active materials or surface modifications of the electrodes, e.g., solid electrolyte interphase (SEI) layer growth [4,9,10]. In the worst case, high temperatures may trigger thermal runaway events, where strongly exothermic reactions cause thermal decomposition of the cell [11]. This phenomenon is usually accompanied by fire and explosion and presents an enormous safety hazard, which must be prevented at any cost.

Temperature is also a fundamental factor when designing battery packs for BEV applications: sets of single battery cells are interconnected to obtain packs that deliver the requested energy and power. In this context, additional challenges related to different cell parameters, such as temperature inhomogeneities, and their impact on pack design and aging behavior need to be considered. In recent years, these points were addressed in several experimental and simulation studies, where according to Baumhöfer et al. [12] variances in materials properties and process parameters may drastically affect the production quality and lifetime of individual cells, revealing that different aging trends significantly influence the performance on pack level. In this context, it is known that in a series connection of cells the weakest cell limits the pack performance. In parallel connected battery strings, outlier battery cells may result in local electrical overloads and cause an accelerated aging behavior of the battery pack [13]. In addition, a non-uniform temperature distribution due to varying ohmic overpotential contributions caused by inhomogeneous current paths was observed in parallel cell assemblies [14], where it was highlighted that dynamic load imbalances linearly increase with the number of cells connected in parallel. Moreover, it was stated that cycling in narrow state-of-charge (SoC) ranges and pulse charging promote nonequal loads and non-uniform cell heating.

Due to the proximity of the cells in the pack configuration, an uncontrolled temperature rise and an inhomogeneous heat distribution within the battery pack may have a dramatic impact on the functionality and safety of the system. Uncontrolled generation of heat is the main driver for accelerated and inhomogeneous pack degradation [15–17]. Therefore, reliable thermo-management and limitation of hotspots within the pack becomes a crucial point to extend the lifetime of the battery pack and maintaining secure operation. Moreover, to comply with the request for ever increasing energy densities in combination with super-fast charging rates for BEVs, the challenge of thermal management grows dramatically.

To precisely control the working temperature of a battery pack, different battery thermal management systems (BTMS) are currently employed in BEVs, which essentially can be divided into four groups, namely 1) air cooling, 2) phase change cooling, 3) liquid cooling and 4) heat pipe cooling systems [18]. Cooling strategies vary from manufacturer to manufacturer: due to its light weight, forced air convection was employed in several BEVs, such as Nissan's Leaf, Renault's Zoe, and Toyota's Prius. In contrast, in the Tesla Model S a patented serpentine liquid cooling technology was realized [19]. General Motor's Chevrolet Volt also uses a liquid cooling system, where coolant passes through cooling plates interwoven with the battery cells, while in the Porsche Boxter E, a computational fluid dynamics (CFD) optimized battery cooling system based on liquid-filled cooling plates was employed [20].

In air cooling systems, the battery cell surfaces are either directly (cooling channels between the cells) or indirectly (cooling plates are placed between the battery cells) exposed to an airflow. Regarding their simple structure, light weight, and low operating costs, this technology appears promising for battery thermal management in automotive applications. Various literature studies revealed that air cooling is suitable for packs with moderate pack sizes [17,21,22]. However, due to the low heat capacity of air (C_p = 1.006 kJ/kg K at standard temperature), air cooling systems require the use of large volumes of air to enable sufficient cooling of battery pack [23]. While Yuksel et al. [24] reported cell-to-cell temperature variances of up to 5 °C in air cooled battery packs, Fan et al. [25] stated that the temperature of the cells may deviate by 10 °C or even more depending on the inlet velocity of the airflow. Air cooling systems were the first choice for thermal management systems of first EVs, mainly due to their simplicity. Nowadays, these cooling systems seem to be no longer attractive and sufficient, and today's EVs are equipped with more effective ones.

Phase change cooling systems may be based on liquid-to-gas or solid-to-liquid conversion materials, respectively. Heat pipes are among the most used liquid-to gas phase cooling systems. During heat transfer a working fluid is evaporated from an evaporator to a condenser and transported back to the evaporator [26]. Compared to air cooling, heat pipes exhibit higher heat dissipation efficiencies, while costs and maintenance effort are on a similar level [27]. Due to these advantages, this passive cooling system has been tested in battery packs for electric vehicles [28]. Despite those promising features, heat pipes are still in development phase and considerable optimization work remains to improve the cooling performance of this technology [18]. Solid-to-liquid conversion cooling systems are commonly referred to as phase change material (PCM) cooling systems. Among the large variety of different PCMs, paraffins are the most promising candidates for lithium-ion battery thermal management applications, as they are non-corrosive, non-toxic, and recyclable. These compounds undergo a solid-to-liquid phase transformation in a low to medium temperature range between 15 °C to 130 °C [29]. Due to their ability to absorb heat during phase change, PCMs can effectively lower the temperature of the battery pack. However, PCMs typically exhibit low thermal conductivities, thus leading to a poor heat conduction of the system.

To overcome the drawbacks related to the cooling technologies presented above, in literature different approaches dealing with the development of hybrid cooling strategies were proposed. In this context, the numerical work presented by Safdari et al. [30] revealed that a hybrid BTMS using a PCM as passive coolant and forced airflow as active cooling component enables excellent thermal management. Another concept utilizing forced-air-flow-enhanced liquid water evaporative phase change to control the temperature of lithium-ion battery modules was suggested by Wei and Agelin-Chaab [31]: results indicates that the concept can improve cooling efficiency and temperature uniformity by more than 70 % compared to concept with no-cooling. To the knowledge of the authors, when writing this work, there are not commercially available applications which are equipped with phase change or heat pipe cooling systems, therefore air cooling and mainly liquid cooling are nowadays still dominant.

In the case of liquid cooling, a possible classification can differentiate between indirect and direct cooling systems. Liquid cooling systems generally show better cooling capabilities as compared with air cooling and phase change cooling systems, due to high thermal conductivity and specific heat capacity of the liquid [26]. In indirect liquid cooling systems, the coolant does not have direct contact with the cells but circulates in a closed loop (heat sink) within the structure of the battery pack. This is because indirect cooling systems use liquids such as dielectric water/glycol solutions, which are obviously incompatible with the voltage of the cells (high thermal and electrical conductivity). Consequently, direct contact between the coolant and the battery components would lead to a short circuit and thus needs to be prevented [32]. In contrast, in direct liquid-cooling systems, the battery pack and the cell themselves are directly immersed in an electrically non-conductive liquid coolant. By fully submerging the battery pack in a liquid coolant, stable temperature uniformity can be maintained, due to the excellent thermal contact between the liquid and the cells [33]. The topic of the effectiveness and feasibility of direct cooling for lithium-ion cells has been handled in the literature by date only until a certain extend. Recently, a comprehensive review manuscript has been published Roe et al. [34]. The authors have conducted an extended

literature review on the topic of immersion cooling. They highlighted that in the past, authors have focuses on different aspects of this topics: simulation of behavior and performance in short-term at cell [35–37] and pack level [38,39] comparing different thermal management against direct liquid cooling; real experiment to assess short-term performance at cell [40] and pack level [41]; effectiveness of direct liquid cooling for inhibiting thermal runaway [42]. All authors have highlighted the improved performance of direct liquid cooling in respect to other conventional thermal management strategies in decreasing temperature inhomogeneities on cell surface or among cells within a battery pack, together with the capability of suppress pack damage due to a single cell thermal runaway. Additionally, Roe et al. in [34] highlight clearly that the literature by date present a significant gap in studying the lifetime performance of systems which are subjected to immersion cooling in respect to conventional cooling design. Regarding the real application, in 2019, XING Mobility presented the world's first immersion-cooled modular battery pack system at The Battery Show in Stuttgart, demonstrating that immersion cooling systems show excellent safety properties, as a reduction of the average temperature within the battery pack and the non-flammability of the coolants suppress thermal runaway events [43,44]. Despite these highly promising features, immersion cooling technologies have so far only been applied in exceptional cases, as they require the use of costly and specific fluids, together with a more complex system. However, they generally exhibit excellent dielectric properties, a very low electrical conductivity, exceptional chemical stability, and the capacity to operate at very low as well as elevated temperatures in aggressive conditions [45]. To our knowledge, only few mobile applications equipped with direct immersion cooling systems are available on the market at the present time [46]. Summarizing, current literature does not address the effect of active immersed cooling on the degradation behavior of battery packs, nor a quantitative comparison between direct immersion and conventional cooling systems can be found.

To evaluate the technical viability and efficiency of active immersed cooling systems in the short and long-term, a thorough analysis and investigation of a battery pack equipped with this cooling concept was performed in this work, which is the first of a series of two papers. Herein, we present the first experimental study on a novel compact immersion cooling system for cylindrical battery cell packs based on the 3M™ Novec™ 7200 cooling fluid [47]. To analyze and quantify the degradation behavior on battery pack level in homogeneous and non-homogeneous temperature conditions, two identical battery packs composed of 25 cylindrical 18650-type cells were cycled using different thermal management strategies, namely air cooling and active immersed cooling. The first paper focuses on analysis on pack level including temperature and current distribution within the two packs as well as aging of the whole packs. Based on these results, a detailed application-oriented discussion is presented, where the trade-off between efficiency, cost, and safety of the different cooling strategies employed in this work is highlighted and evaluated. The second part of this paper series will focus on how different pack cooling strategies affect the degradation behavior of single cells contained in a parallel battery assembly. To do so, parameterization tests before pack assembly and after pack disassembly are carried out to investigate the functionality and the aging state of the individual cells. In addition to that, the characterization of some of the cells by means of differential analysis and post-mortem analysis allows for the identification of the most relevant aging processes and their relation to the presence of temperature gradients inside the battery pack. The presented two-paper structure put the focus of the first part in understanding the implications of the usage of such cooling strategy (immersion cooling in respect to air cooling) in applications, and what does it means not only in the short-term (performance) but mainly in the long-term (aging) operation. The understanding of the cells behavior during aging when subjected to the two different cooling strategies and the explanation of the identified phenomena within the experiment is then shifted to the second paper, focusing more on understanding of degradation.

The remainder of this paper is structured as follows: in Section 2 the construction of the battery pack and the experimental setup applied for the investigation of the different cooling systems will be described. Furthermore, the design of an active immersion cooling system is addressed, which provides the framework for efficient thermal management of battery packs. Moreover, an overview of the testing procedures employed in this work is given, which builds the foundation for the experimental results presented in the subsequent Section 3. Within this section, also a technical and economical discussion oriented to application of such a cooling strategy is presented. Finally, Section 4 provides concluding remarks and gives an outlook for future investigations.

2. Experimental

2.1. Pack design and cell type

To test and quantitatively compare different cooling strategies, two battery packs being composed of 25 cylindrical Li-ion cells of type SONY US18650VTC6 [48] were designed. These cells combine an NMC-based cathode with a graphite anode and exhibit a nominal capacity of 3 Ah and a nominal voltage of 3.6 V, while the maximum constant charge and discharge currents are 5 A and 30 A, respectively. The choice of employing this type of cell for such investigation is only based on the high market availability and rather good production quality and is not related to the optimal performance in a certain application. Before pack assembly, the single cells weight and open circuit voltage (OCV) were collected. An average weight of 46.73 g with a standard deviation of 0.09 g was calculated. All weights fell in the range between 46.6 ± 1.5 g as specified in the technical data sheet of the cell manufacturer. The OCVs were distributed around 3.48 V, thus corresponding to the 75 % discharge state shipping requirement. In addition to that, the 1 kHz AC resistance of the cells was determined, where a mean value of 12.96 mΩ was measured (standard deviation 0.15 mΩ). To guarantee all cells were of the same acceptable quality, an initialization test (check-up) on cell level was performed for all samples. The test included subsequent charging and discharging of the cells at a C-rate of 1C and 0.1C, and a pulse test at three different SoCs to estimate internal cell resistance by means of the following equation:

$$R_i(t) = \frac{V(t) - V(t=0)}{\frac{1}{\Delta t}\sum_{i=1}^{t} I(i)} \tag{1}$$

Here, V corresponds to the cell voltage, I is the applied current, and Δt is the considered pulse duration. For simplification, the pulse resistance measured after a duration of 0.5 s is defined as the internal resistance of the cell. In fact, within the employed testing equipment, this value comes closest to the so-called real internal resistance. All 50 cells tested have shown limited statistical deviation for the considered parameters. The standard deviation of the measured 1C capacities was less than 0.5 % of the mean value (around 3.039 Ah), which is exceptional low. For the internal resistance measured at 50 % SoC the standard deviation is approx. 1.7 % of the mean value (18.3 mΩ), which is significantly higher than the one related to the capacity. At 100 % and 10 % SoC the variance slightly increases, which is a normal expected behavior. The check-up results reveal that the cells under investigation were characterized by similarly high-quality standards and thus have proven to be suitable for application in the present study. The battery packs built in this work were designed in a square format containing a 5 × 5 cell matrix, as shown in Fig. 1.

The side length of the pack is 10 cm. Suitable spacers were introduced to ensure a 0.5 cm distance between two cells. The pack height is 6.6 cm, which basically equals the height of an 18650 cell, thus underlining the space-saving design of the pack. To evaluate the measurement data, the cells within the pack are divided into five position-

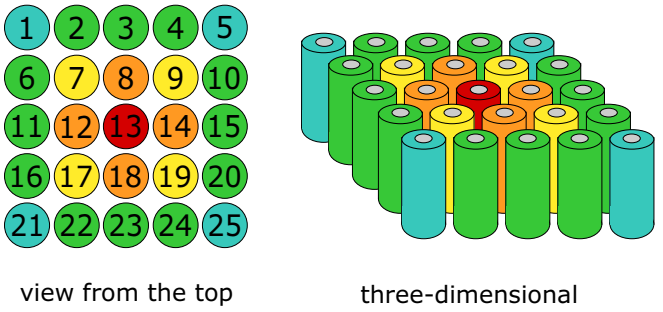

Fig. 1. Positioning of cells and definition of measurement groups.

dependent groups, which vary in their capability to dissipate heat into the environment. The groups are marked by different colors, as indicated in Fig. 2. In the following, these groups will be labelled according to their position acronyms defined in Table 1.

All cells are connected in parallel. This results in a total nominal pack capacity of 75 Ah and a nominal voltage of 3.6 V. As parallel connected pack where the cells are forced towards the same voltage level, the single cell current measurement is of high importance. Therefore, the current of each cell was individually recorded by a single shunt. Additionally, the cell temperatures, the pack voltage, and the pack current were measured. The measurement setup is schematically depicted in Fig. 2.

The pack current and the single cell currents are measured at the positive pole of the cells. For this purpose, the INA226 sensor from Texas Instruments is used. Its maximum shunt voltage gain error is 0.1 %. With the same sensor, the total pack current is measured, but replacing the 1 mΩ shunt by a LUMEL 60 mV-150 A shunt (accuracy class 0.2). Initial deviations in the measured values were controlled by sensor calibration. Cell temperature measurements were performed using Maxim Integrated DS18S20 temperature sensors (work temperature range of −55 °C to +125 °C). In a temperature range between −10 °C to +85 °C the sensors operate with an accuracy of ±0.5 °C. The position of the temperature sensors is indicated by the orange/red semicircles in Fig. 2. Due to the limited space inside the pack, each cell is equipped with a single sensor located at the center of the lateral surface of the cell, fixed with a thermal conductive glue. It is important to note that the temperature measured in this way may deviate from the real surface temperature of the cell, since the sensing unit is facing the cell surface only with one side, while the other side is pointing away from it, thus resulting in a measured mix-temperature. In addition to that, all sensors are pointing to the same direction, irrespective of the position of the cell within the battery pack. Consequently, some sensors point into the pack, while others are oriented outwardly. Due to these variations, a precise measurement and quantitative analysis of the cell temperature is considered as not completely reliable. Instead, the temperature values detected by the sensors allow to draw conclusions about qualitative temperature trend and distribution within the pack. To facilitate a comparison of the different cooling systems, the two battery packs employed are constructed in the same way. Data processing of the digital signals and measurement of the analogue voltage was performed using a T7Pro data logger (LabJack). As the total voltage of the battery module varies between 2.5 V and 4.2 V a measurement range of ±10 V was selected, with accuracy of ±0.01 %.

To provide stable resistances, the length of the cables in the measurement setup was kept constant. Moreover, when installing the cables on the conductor rails, it was ensured that the current paths in all strings were of the same length. To keep the resistance of the device as small as possible, a cable of minimum length and with the largest cross section of 1.5 mm^2 was chosen. Although resistances due to the measurement device and extended cables were minimized, they still have a non-negligible influence on the measurement and were therefore considered in the development of the testing procedure presented in Chapter 2.3.

2.2. Cooling set-up

As mentioned, two different packs of same capacity size are assembled with two different cooling systems. The two configurations are represented in Fig. 3. Some real picture can be found in Fig. S1 of the supplementary material. The first pack configuration is represented in Fig. 3a): it is cooled with forced air circulation inside a climate chamber, and it will be from now on indicated as Pack A. In this case, the term force cooling refers to the effect of force air circulation inside the climate chamber by means of an integrated fan. In Fig. 3a) the green arrows represent possible flow paths for air circulation. The second pack configuration is schematically represented in Fig. 3b): it is cooled by mean of a novel active immersion cooling system based on the 3M™ cooling liquid Novec™ 7200 [49]. The pack will be indicated from now on as Pack N. This non-flammable, volatile high-tech liquid is thermally stable and exhibits a negligibly low electrical conductivity. Its density of 1.5 g/cm^3 exceeds that of water by one half, while its boiling point is at 76 °C. Moreover, Novec™ is an excellent heat conductor.

As schematically shown in Fig. 3b), the cooling system of Pack N is composed of a sealed liquid tank, a radiator, and circulatory tempering unit. The battery pack is installed in the sealed liquid tank, filled with the Novec™ coolant up to the level at which the pack is fully immersed in the liquid. In addition to that the cooling unit contains the radiator, which is in direct contact with the Novec™ coolant. Actively cooled water enters the radiator from an external water tank through the water inlet and flows back to the external tank through the water outlet, where

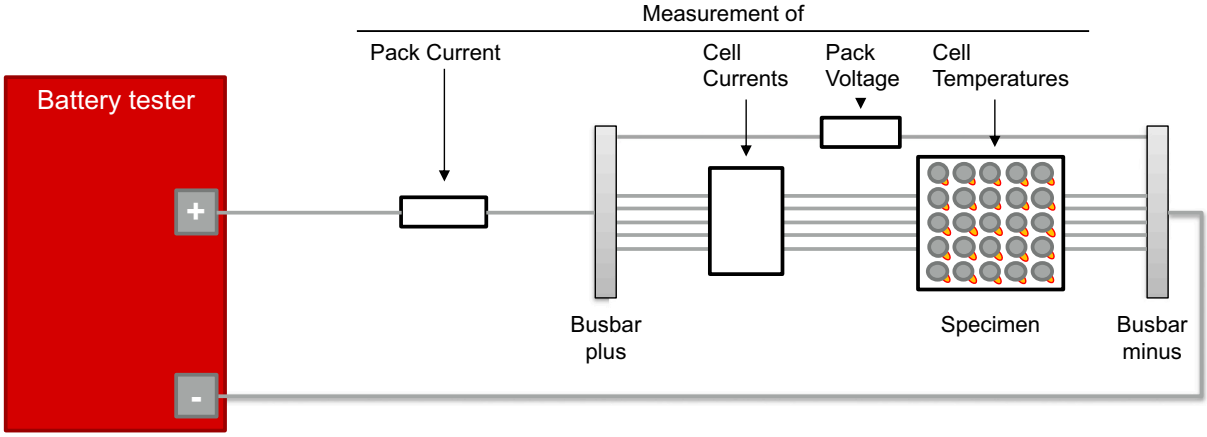

Fig. 2. Schematic presentation of the measurement setup.

Table 1
Color and position dependent naming of cells due to their ability to dissipate heat.

Color	Cyan	Green	Yellow	Orange	Red
Position (acronym)	Outer Corner (OC)	Outer (O)	Inner Corner (IC)	Inner (I)	Center (C)
Cells	1, 5, 21, 25	2, 3, 4, 6, 10, 11, 15, 16, 20, 22, 23, 24	7, 8, 17, 19	8, 12, 14, 18	13

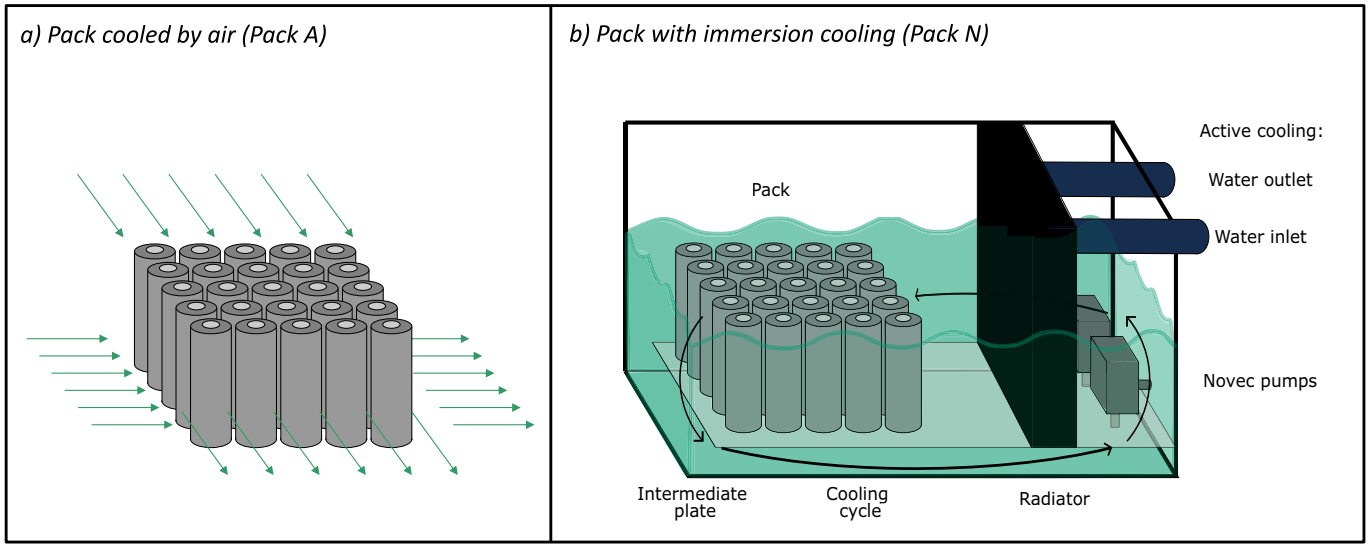

Fig. 3. Representation of the cooling setup for the two different experiments, a) pack cooled by air (Pack A), b) pack with immersion cooling (Pack N).

the flow rate of the water pumped through the radiator is 4.2 l/min. To obtain a homogeneous distribution of heat inside the system, the Novec™ cooling liquid is actively tempered using a circulatory cooling unit, which is composed of an intermediate plate and two pumps. The coolant is pumped through an inlet into the intermediate plate, where the maximum flow rate is 3.67 l/min. The outlet is directed towards the wall of the sealed container, to force convection of the Novec™ coolant, which circulates between the cells and the radiator, where a heat exchange occurs, thus resulting in an optimum dissipation of heat within the system.

2.3. Cycle testing procedure

To force accelerated aging by means of temperature increase, the pack was continuously cycled at a charging and discharging current rate of 1.33C (100 A), between minimum and maximum pack voltage of 2.5 V and 4.2 V respectively.

As only the pack voltage can be measured, the single cells are cycled in a smaller voltage window, which depends on different factors, such as cable length, cell internal resistance, cell contacts and single cell degradation. As mentioned before, the setup is built in a way that the contribution of cable length is limited as much as possible for both packs. The present state of the cells was controlled by conducting regular check-up tests (1st cycle and then every 75th cycle) until the end-of life criterion of 80 % SoH was reached. A detailed overview of the different steps applied during the check-up test is provided in Table 2. The check-up procedure starts with a five-hour break, thus allowing the system to cool down and settle in its steady state. Using a standard constant current-constant voltage (CCCV) charging procedure, the pack is then charged for a maximum time of 2.5 h with a constant current of 75 A and an upper voltage limit of 4.2 V. Afterwards, a 1C capacity check is performed by employing a standard discharge procedure, in which a constant discharge current of 75 A is applied until the end-of-discharge voltage (EODV) of 2.5 V is reached. After a full charge procedure, the pack is discharged following the standard procedure, where a pulse of 10 s at 1C is carried out at 80 %, 50 %, and 20 % SoC respectively. The check-up procedure terminates with a 0.1C capacity check.

Table 2
Detailed check-up procedure.

Step	Operator	Nominal value	Limit	Information
1	Break		5 h	
2	Standard charge procedure	75 A, 4.2 V	2.5 h	
3	Break		30 min	
4	Standard discharge procedure	75 A	2.5 V	Definition of pack capacity C_{actual}
5	Standard charge procedure	75 A, 4.2 V	2.5 h	
6	Discharge	75 A	−20 % C_{actual}	80 % SOC
7	Break		30 min	
8	Discharge pulse	75 A	10 s	
Repeat Steps 6–8 with ΔSoC of 30 % to reach 50 % SoC and 20 % SOC				
9	Standard charge procedure	75 A, 4.2 V	2.5 h	
10	Discharge	7.5 A	2.5 V	

3. Results

The following section provides a comprehensive insight into the aging tests performed on the two battery packs equipped with the different cooling systems. To ensure the comparability and functionality of both samples and testing setups, the initial condition of the single cells and the packs assembled were characterized by means of the first check-

up test. Next, the degradation behavior of the packs is analyzed over the entire runtime of the experiment, where a special focus is placed on the capacity evolution on pack and cell level.

3.1. Beginning of life

As mentioned in Section 2.1, before pack assembly, check-up tests were performed on each individual cell to validate their functionality. Afterwards, the cells were connected in parallel under the 5 × 5 cell configuration according to the procedure described in Section 2.1, thus resulting in the generation of two identical battery packs. The packs were equipped with the different cooling systems and subsequent check-up measurements were carried out to compare pack performance. Fig. 4 presents exemplary voltage curves and current profile of the different setups as well as the temperature variation of the cells contained within the different packs during a check-up test. From Fig. 4a it becomes obvious, that almost identical voltage curves emerge irrespective of the cooling system applied (maximum voltage difference of approx. 10 mV at around 2.5. However, after the first 1C discharge step, Pack N relaxes to a slightly higher steady state voltage level in respect to Pack A. Moreover, evidently during the discharge/charge process under 1C current rate, the temperature values detected for the cells contained in Pack N strongly differ from those recorded for the cells cooled by air-cooling. In both cases, the temperature of the cells is position-dependent and increases from the outside to the inside of the pack, where at the point of complete discharge maximum temperature values of 26 °C and 40 °C were detected for the cells located at the center of Pack N and Pack A respectively (approx. after 2–2.5 h the test started). In addition, at this point the largest temperature variation between individual cells contained in the same pack configuration can be observed. While in Pack N the temperature difference between the cells exhibiting the lowest and the highest temperature is only 3C°, in Pack A the difference in temperature is 16 °C. In contrast, during the discharge/charge process under 0.1C current rate, the temperature of all cells is virtually identical and remains rather constant throughout the charge/discharge cycle, irrespective of the cooling system applied.

Table 3 gives an overview of the capacity values delivered for the two packs during the 1C and 0.1C current rate discharge process of the first check-up test. Additionally, the respective output capacities measured for the single cells contained in the different packs were summed up. Moreover, the table shows the ratio between the measured and the calculated pack capacities.

During the discharge process under 1C current rate, the measured output capacity of Pack A exceeds that of Pack N by 0.7 Ah (approx. 1 %

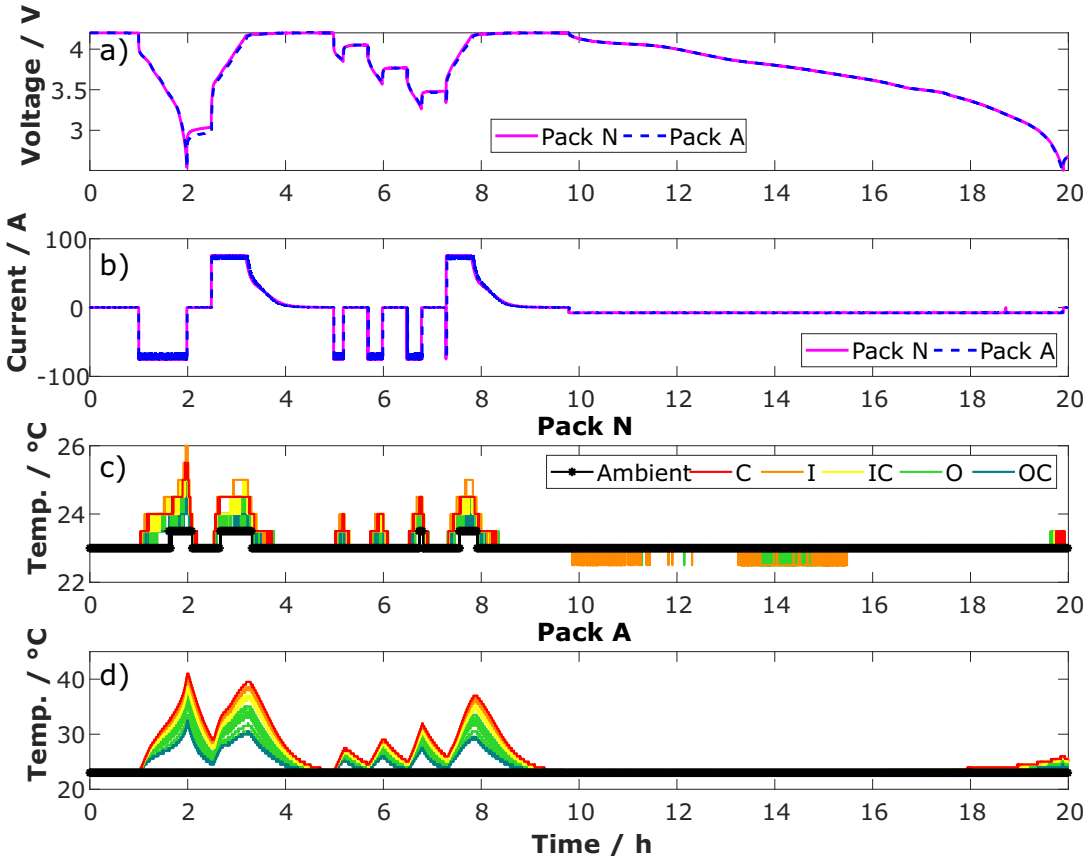

Fig. 4. Comparison of first check-up test. a) shows the voltage curve of both packs. b) shows the employed current profile. c) and d) display the temperature of Pack N and Pack A. The legend is valid for all cells of one position type (OC = Outside corner, O = Outside, IC = Inner corner, I = Inner, C = center as indicated in Table 1). Please note the different temperature scale for the plot c) and d).

Table 3
Capacity throughput during first check-up in Ah. "∑ cells" stand for cumulation of all individual cell capacities from initial Check-Up.

Capacity	1C			0.1C		
	Pack	∑ cells	Pack/∑ cells	Pack	∑ cell	Pack/∑ cells
Pack N	73.71 Ah	76.29 Ah	96.11 %	75.86 Ah	77.45 Ah	98.00 %
Pack A	74.4 Ah	75.69 Ah	98.30 %	75.62 Ah	77.1 Ah	98.08 %

of the nominal capacity). In contrast, during the discharge process under 0.1C current rate, the capacity of the Pack N is slightly higher than that of Pack A, where this difference is practically negligible. This behavior is in good agreement with the temperature variation observed for the cells contained in the two packs. As outlined above, during 1C discharge, the overall temperature of Pack A is much higher than that measured for Pack N. At higher temperatures, internal battery resistances, such as the electrolyte and the charge transfer resistances are smaller. According to Ohm's law, the voltage drop observed at the beginning of the discharge step is directly proportional to the internal battery resistance. Accordingly, at higher temperatures the voltage drop decreases. The lower the voltage drop, the higher is the capacity throughput of the cell. Consequently, the air-cooled pack reaches higher capacity values during 1C discharge. In contrast, during 0.1C discharge, the low current rate does not considerably affect the temperature of the cells, such that almost identical temperature and capacity values are recorded for the two pack configurations. Due to its higher internal resistance (temperature effect), Pack N reaches the cut-off voltage faster than Pack A. Therefore, at 2.5 V the SoC of Pack N does not attain the state of full discharge but exhibits an SoC larger than 0 %. As a result, during relaxation the steady state voltage-level of Pack N slightly exceeds that of Pack A (Fig. 4a).

Contrary to what was observed for the measured pack capacities, the capacity calculated from the single cells of Pack N is higher than the cumulated capacity of Pack A, where this behavior is again more pronounced during discharge at 1C. Irrespective of the current rate applied, for both packs the capacity values measured from the single cell capacities are higher than the capacities measured after pack assembly. When looking at the ratio of measured and calculated capacity values it becomes obvious that the real capacity measured for Pack N at 1C reaches only 96.11 % of the cumulated value, while the measured capacity of the Pack A reaches 98.3 % of the cumulated value. At 0.1C, the ratio between the measured and the calculated capacity yields a value of approximately 98 % for both packs. This behavior could be due to an inhomogeneous current distribution between cells. In non-ideal battery packs, the variation in internal resistance values between the different cells leads to varying individual cell currents. Consequently, some cells reach their cut-off voltage earlier than others, thus limiting the deliverable output capacity of these cells. This effect becomes particularly dominant when the applied current rate is high.

3.2. Degradation analysis at pack level

In the following sections, the aging behavior of the battery packs equipped with the two different cooling systems is discussed. Different key figures, such as temperature and current distribution, capacity evolution, internal resistance and total Ah-throughput are presented and analyzed in detail.

3.2.1. Temperature development over cycles

In Fig. 5a) and b) the temperature variation of the 25 cells contained within Pack A and Pack N, respectively, is presented over the entire testing time. The cells are marked according to the position-dependent color scheme introduced in Section 2.1. Moreover, the figures show the corresponding ambient temperature curves (black). For the air-cooled setup an ambient temperature of 23 °C was recorded, which remained virtually constant throughout the entire runtime of the experiment. In contrast, the ambient temperature of Pack N slightly varied between 23 °C and 24.5 °C, forming a periodically repeating pattern. This behavior reveals that the temperature of the cooling liquid into which the cells are immersed slightly deviates from the targeted ambient temperature value due to heat absorption/dissipation during cycling.

The temperature of the cells contained in Pack N varies in a range between 22.5 °C and 26.5 °C (observed throughout all the testing profile), where the average temperature inside the pack, which was derived from the mean temperature values of all 25 cells, is slightly higher during the cycling sequence than during the check-up procedure (approx. 24.5–25 °C during cycling against 23–23.5 °C during check-up). During cycling, the difference between the maximum and minimum cell temperature recorded for the cells located at the center (C) and at the outer corners (OC) of the battery pack, respectively, is approximately 3 °C. In agreement with the results presented in Section 3.1, the

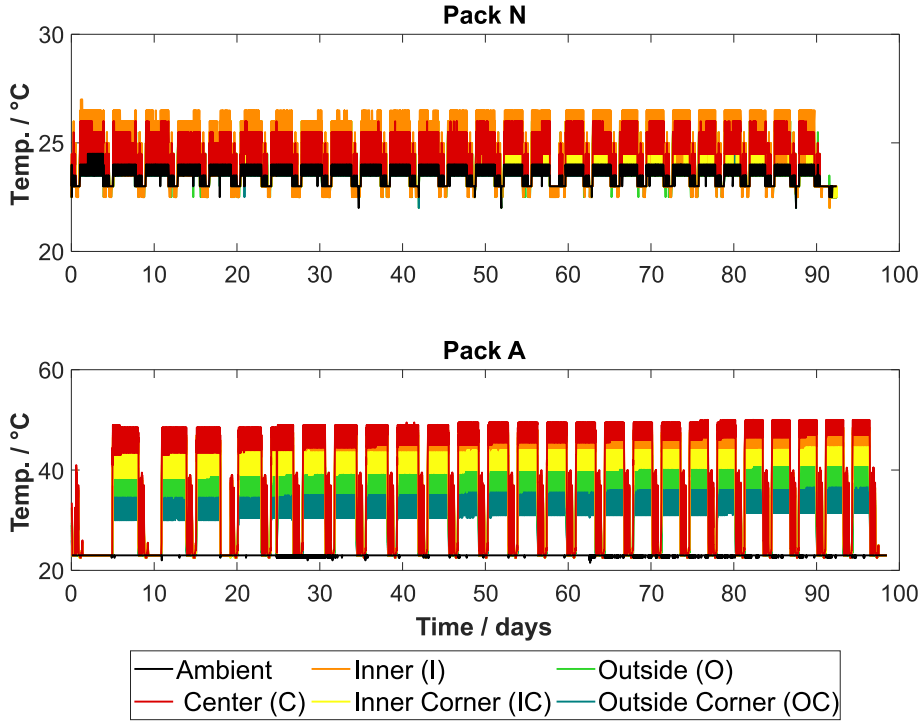

Fig. 5. Temperature development of both packs over total run time in days. Each subplot shows 26 curves considering the ambient temperature, whereas their coloring is position dependent (refer to Table 1). Please note the different temperature scale.

temperature of the cells decreases with increasing distance from the center of the pack, however, the temperature values of the inner (I) cells, the inner corner (IC) cells, and the outer (O) cells are almost identical. Therefore, the temperature curves corresponding to these cells overlap and cannot be visually distinguished.

As expected, the cells contained in Pack A show a more inhomogeneous temperature behavior. During the cycling sequence, the minimum temperature measured for an OC cell is approx. 30 °C at the beginning of the test and 31.5 °C towards the end of the test, while a maximum temperature of 48.5 °C at the beginning of the test and 50 °C towards the end of the test is recorded for the cell located at the center of the battery pack. Consequently, the temperature range in Pack A is almost seven times larger than the one observed for Pack N and the temperature variation between the cells located at the different positions of the pack can be clearly distinguished. Here, it must be noted that on day 25, Pack A was accidentally cooled down to room temperature for a short period of time during the cycling sequence, due to an unwanted test interruption. However, this should not lead to any appreciable changes in the long-term degradation behavior and the observed temperature trend of the battery pack.

To summarize, the temperature of the cells contained in Pack A show dramatic temperature variations. Especially, the cells located in and around the center of the battery pack reach high, safety-critical temperatures, caused by the poor dissipation of heat inside the battery pack. Moreover, the temperature of the cells slightly increases with increasing testing time, irrespective of the position of the cells. In contrast, the Novec™ cooling liquid allows for more efficient heat dissipation, which only results in small temperature variations between the cells located at different positions inside the pack, where the temperature variation of the cells corresponding to the same position-dependent group is highly homogeneous over the entire measurement.

3.2.2. *Pack capacity evolution*

In this section, the aging behavior of the battery packs is examined. The SoH of the battery pack can refer to its present capacity (SoH_C) or to its internal resistance (SoH_R). In this work, only the SoH_C is considered to directly represent the degradation behavior of the battery pack. This is calculated as the ratio between the actual pack capacity and its initial discharge capacity. Therefore, the capacity values recorded during the check-up tests are analyzed more in detail.

The pack capacity was determined during the 1C discharge step, which was performed according to the testing procedure outlined in Section 2.3. Fig. 6a) shows the absolute capacity values measured for the two different battery packs as a function of equivalent full cycles (EFC). One EFC corresponds to 150 Ah. In Fig. 6b), the variation of the corresponding relative capacities, calculated from the ratio of the consecutively measured capacity values and the initial pack capacity (SoH_C) is depicted. As explained in Section 3.1, the pack capacities determined during the first check-up test show a deviation of approximately 1 % from their nominal capacity values, where the initial absolute capacity of Pack A exceeds that of Pack N due to the higher pack temperature, which results in higher capacity values. However, the absolute capacity values of Pack A drop much faster than those related to Pack N. The same trend is observed for the relative capacity values. In this case the initial SOH_C value of both packs is equal to one. For Pack A, the end-of-life (EoL) condition of an SoH_C lower than 80 % is met after a total Ah-throughput of approx. 125 kAh and 840 equivalent full cycles, while Pack N reaches its EoL criterium at approx. 154 kAh and 1025 equivalent full cycles. The larger capacity losses observed for Pack A can be explained evidently by higher pack temperatures, which result in accelerated aging processes. Here, it must be stressed that both packs were cycled under different conditions. For Pack N, lower pack temperatures result in higher internal resistances of the cells contained within the battery pack. Therefore, the cut-off voltage of the pack is reached before the cells are fully charged/discharged, thus resulting in a lower Ah-throughput as compared to Pack A. During the first cycling sequence, Pack N shows an Ah-throughput of 6.95 kAh while that of Pack A equals 7.61 kAh. This effect can also be observed in Fig. 6. The distance between the points at which the pack capacity was determined is smaller for Pack N than for Pack A. This means that during the runtime of the experiment Pack N experiences more check-up cycles and thus longer rest periods than Pack A. Consequently, Pack A is exposed to higher loads, which may also affect its degradation behavior.

Although different cycling conditions could have been avoided by applying current-based charging/discharging limits (i.e., cycling against same depth-of-discharge or DoD) instead of voltage-based charging, the experiments were setup more with the aim to create application-oriented testing scenarios under close to real-life conditions. In

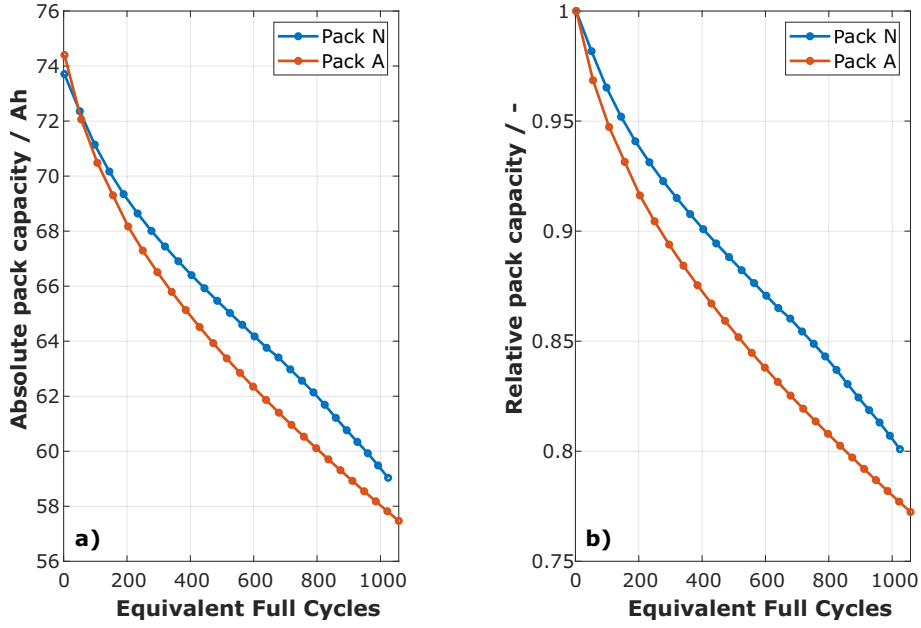

Fig. 6. Capacity trend at 1C rate of both packs over equivalent full cycles at each check-up, a) absolute capacity trend and b) normalized capacity trend in respect to initial measured values for each pack.

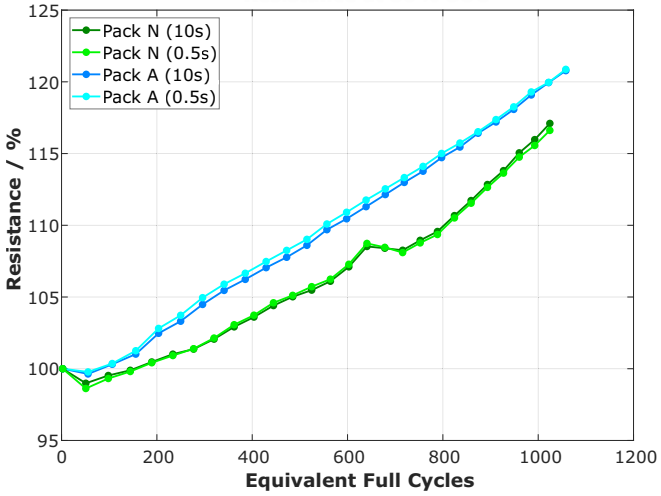

Fig. 7. Internal resistance calculated after 0.5 s and 10s for both packs at 50 % SoC.

addition to that, it is important to note that the capacity curves detected for Pack A exhibit the commonly expected exponential shape. In contrast, the capacities measured for Pack N initially follow an exponential decrease until a cycle number of about 400 EFC is reached, where a linear course arises up to cycle 770 (loss of capacity of approx. 11.2 mAh/EFC or 0.015 %/EFC), which finally change its slope increasing the aging rate (loss of capacity of approx. 13.2 mAh/EFC or 0.018 %/EFC). This behavior will be discussed more in detail in the following subsection and in Section 3.3.

3.2.3. Pack internal resistance development

The internal pack resistances give additional information about the aging behavior of the packs. Fig. 7 shows the resistance values that were calculated according to Eq. (1) at 50 % SoC after 0.5 s and 10 s pulses, respectively. Interestingly, for both packs the second resistance value, which was determined during the second check-up test, is lower than the initial value, which was defined as 100 %. Subsequently, the resistance values of the packs increase in an almost linear manner. In both cases, similar pack resistances emerge irrespective of the duration of the pulses. However, when comparing both packs, the resistance values determined for Pack A reach higher values than those of Pack N. At the EoL of the battery packs, the internal resistance of the Pack N raised by 17 % at 50 % SOC, while that of Pack A raised by approximately 21 %. This observation matches the results outlined in earlier sections and again reflects the accelerated degradation behavior observed for Pack A. Similar results can be obtained observing the behavior of the internal resistance at 80 % and 20 % SoC which can be found respectively in Fig. S2 and Fig. S3 of the supplementary material.

3.2.4. Current distribution

Due to the pack configurations (parallel connections), the currents of single cells might show large deviations: in fact, when the cells are forced to have the same voltage, differences in cell internal impedance (e.g., due to temperature distribution or different degradation) lead to differences in cell current. An exemplary behavior of the single cells pack performance during the degradation procedure for the two pack setups is reported in Fig. 8. The proposed behavior is referred to the discharge process with constant pack current of 100 A at cycle number 450 and shows the single cell current behavior for the Pack N (Fig. 8a) and for the Pack A (Fig. 8b) and the single cell temperature behavior for the Pack N (Fig. 8c) and for the Pack A (Fig. 8d) respectively. On the one hand, it can be noticed that the temperature distribution of Pack N (Fig. 8c) is rather uniform among the cells, remaining in a range between approx. 23.5 °C and 26 °C. On the other hand, the temperature distribution of the cells in Pack A (Fig. 8d) show a visible and clear spread, ranging from a minimum of 30 °C in the middle of the discharge process up to approx. 48.5 °C and 47 °C at the beginning and the end of the discharge process respectively. This kind of bath form of the temperature behavior is related to the parabolic shape of the resistance vs. SoC curve shown by this cell, which is characterized by slightly higher

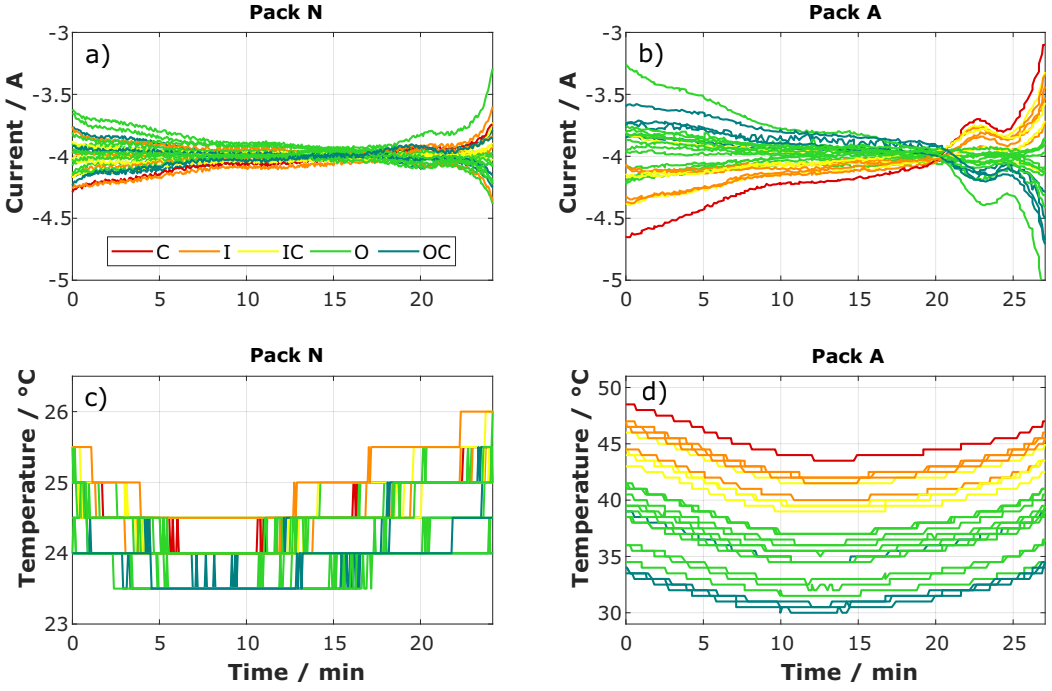

Fig. 8. Example of current distribution (a and b) and temperature (c and d) for the individual cells of the pack during discharge step of cycle 450 for the Pack N (a and c) and Pack A (b and d). In the legend: OC = Outside corner, O = Outside, IC = Inner corner, I = Inner, C = center. Note the different temperature scale of the figures c) and d).

internal impedance in the high and low SoC ranges in respect to the middle range. The described temperature trends evidently reflect the expected behaviors of both packs due to the different cooling systems, and directly influence the current distributions among the cells. As displayed in Fig. 8a for the Pack N and in Fig. 8b for the Pack A, the current distribution shows a similar qualitative behavior, which can be divided in three phases:

1. In a first phase, an evident current spread is visible in a range between −4.29 A and −3.62 A (difference of 0.67 A) for the Pack N, and in a range between −4.65 A and −3.27 A (difference of 1.38 A) for Pack A respectively.
2. After approx. 10 min, the current spread is reduced for both packs, where at a time around 15 min values in a range between-4.07 A and −3.92 A (difference of 0.15 A) for Pack N and in a range between −4.17 A and −3.82 A (difference of 0.35 A) for Pack A are measured respectively.
3. A third phase starts at a time around 20 min, where current spread starts again to increase reaching the maximum deviation between maximum and minimum at the end of the discharge process. In these conditions, values in a range between −4.38 A and −3.29 A (difference of 1.09 A) for Pack N and in a in a range between −5.31 A and −3.10 A (difference of 2.21 A) for Pack A are measured respectively.

This kind of behavior, which qualitative is presented for both packs, it can be observed throughout all lifetime and can be simply explained as following. The battery pack voltage can be modeled according to Eq. (2) considering a simple equivalent cell model for each cell with one single battery internal resistance:

$$V_{pack} = V_{cell,i} = V_{OCV,i} + R_{cell,i} * I_{cell,i} \quad (2)$$

where V_{pack} represents pack voltage, which in this case corresponds to the single cell voltage for the *i-th* cell $V_{cell,i}$, $V_{OCV,i}$ represents the open circuit voltage (OCV) for the *i-th* cell, $R_{cell,i}$ and $I_{cell,i}$ are respectively the internal resistance and the current for the *i-th* cell. If we simply consider two cells in a fully charged state connected in parallel with the same open circuit voltage V_{OCV}, the cell with the lower internal resistance R_{cell} draws a proportionally higher cell current I_{cell} as soon as the cells are discharged. The OCV of the cell that draws the larger current changes faster. Considering

- the typical internal resistance dependency from the SoC ("bath" or U-shaped curve, with higher resistance values in the low and high SoC range [50,51]), and
- the nonlinear relation of open circuit voltage vs. SoC of NMC-based cells (especially in low SoC region)

in the middle SoC range both cells will have very similar resistance values if they are not aged dramatically different. At a certain point, the cell which at the beginning drew more current due to lower resistance will reach lower SoC range faster, with then higher internal resistance. Therefore, the current distribution between the two cells is now reversed. The phenomena is studied by several researchers [6,17,21,27] and is observed at the same manner also for the presented pack configuration, as shown in Fig. 8d) more evidently: at the beginning of the discharge process, the cell with the highest current is the one in the center of the pack (in red), which at the end of the discharge process results as the cell which draws the lowest current.

3.2.5. Capacity degradation

Fig. 9 shows the capacity evolution during the degradation process for the two battery packs. Fig. 9a) and b) present the development of discharge capacities of each single cell for all discharge cycles under 1.33C current over the total charge/discharge throughput for Pack N and Pack A respectively. The corresponding temperature behavior is depicted in subplots Fig. 9c) and d). The capacity of each 1.33C discharge step is calculated by integrating the current values. The temperature values show the average temperature of each discharge step. Due to the chosen test procedure, i.e., how the battery packs are cycled, the measured available battery capacity is significantly reduced with respect to the total single cell full discharge capacity. Table 4

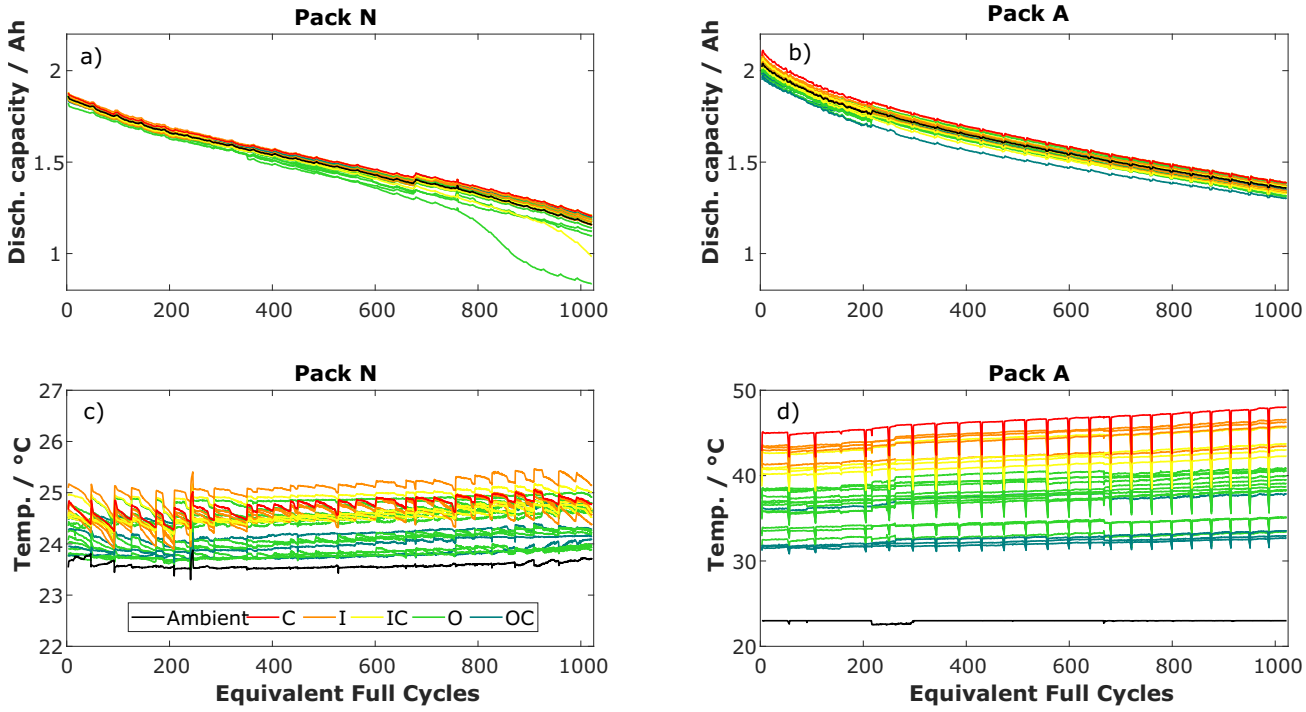

Fig. 9. Evolution of discharge capacity (a and b) and temperature distribution (c and d) during cycling over equivalent full cycles for pack N (a and c) and pack A (b and d). In the subplot a) and b) the black line identifies the average behavior of the pack. Note the different temperature scale of the figures c) and d).

Table 4
Values of the measured maximum capacity, minimum capacity, difference between minimum and maximum capacity (ΔAh) and average capacity at the beginning of test, after 500 EFC and at the end of test for both packs.

Ah-throughput/Ah		Pack N	Pack A
Beginning of test	Max	1.883	2.110
	Min	1.832	1.962
	ΔAh	0.051	0.148
	Average	1.861	2.040
At 500 EFC (approx. middle of test)	Max	1.513	1.638
	Min	1.430	1.513
	ΔAh	0.083	0.125
	Average	1.487	1.596
End of test	Max	1.211	1.387
	Min	0.8367/1.100	1.299
	ΔAh	0.374/0.111	0.088
	Average	1.157/1.178	1.356

presents the results for both packs in terms of maximum capacity, minimum capacity, difference between minimum and maximum capacity (ΔAh) and average capacity at the beginning of the cycling test, after 500 EFC (an Ah-throughput of 75 kAh approx. middle of test) and at the end of test. Considering firstly the Pack A, as it can be seen exemplarily in Fig. 9b, the maximum and minimum extractable capacity at the beginning of test (as reported in Table 4) in the present cycling conditions is approx. 70 % and 65 % of the nominal single cell capacity, respectively.

Approximately 10 % of this total capacity is unavailable due to cabling losses, the rest can be attributed to the cell impedances (function of present temperature) and the parallel connection.

At the end of test, the maximum and minimum extractable capacity is approx. 46 % and 43 % of the nominal single cell capacity, respectively. Moreover, a rather high deviation between the maximum and minimum capacity of approx. 0.148 Ah at the beginning of life is detected, where this value tends to decrease slightly during lifetime, reaching at middle of test 0.125 Ah and at the end of test 0.088 Ah. While this deviation can be attributed to the high temperature distribution, it seems that this behavior is rather maintained throughout the entire lifetime, showing a certain unexpected homogeneity in degradation, i.e., cells follow all the same qualitative aging trend. Looking at the temperature distributions shown in Fig. 9d, a temperature deviation of 13.25 °C between the maximum and minimum temperature is measured. At the beginning of test, maximum and minimum cell temperature are respectively 44.95 °C and 31.7 °C. As soon as the pack ages, an increasing temperature trend can be noted: at the end of the test, a temperature deviation of 15.3 °C between the maximum (48 °C) and minimum (32.7 °C) temperature is measured.

Looking at the results obtained for Pack N (Fig. 9a), the maximum and minimum extractable capacity at the beginning of test (as reported in Table 4) in the present cycling conditions is approx. 62 % and 61 % of the nominal single cell capacity, respectively. Until approx. 350 EFC, the pack maintain a rather uniform aging behavior: at this point, the maximum and minimum extractable capacity are approx. 1.59 Ah and 1.54 Ah, i.e., circa 53 % and 51 % of the nominal single cell capacities, respectively. Starting from this point at least two cells of the pack (cell number 7 [IC] and cell number 22 [O]) experience a clear capacity deviation with respect to the other cells, which becomes particularly evident at the end of the test. Due to this, the maximum and minimum extractable capacities are approx. 40 % and 27 % of the nominal single cell capacity. If the two mentioned cells are excluded from the calculation, then minimum capacity results in approx. 36 % of the nominal single cell capacity. The reason why these cells experience a different degradation behavior might be related to different reasons. One could be cell quality, which could have generated samples with defects. Other possibility could be related to the setup of the experiment with immersion cooling, which could generate some modifications on the cells, e.g., intrusion of liquid inside the cells. Eventually, possible additional degradation mechanisms such as lithium plating might have appeared in some of the cells. These hypotheses will be verified in the second part of the paper, where an aging analysis based on differential voltage analysis will be carried out, together with possible post-mortem analysis of chosen samples. It is in any case clear that the presence of at least one cell, which behaves as outlier, generates decompensation for the other healthier cells. This means in turns that these cells must compensate in terms of currents the weaker ones. Therefore, the pack degradation at the end of the test results in wider spread of capacity between all cells. In fact, considering the beginning of test, in comparison with Pack N, the deviation between the maximum and minimum capacity is factor three smaller (0.051 Ah against 0.148 Ah). At middle of test, this deviation increases slightly for Pack N (0.083 Ah) in respect of beginning of test, which shows an opposite trend in respect to Pack A (0.148 Ah and 0.125 Ah at beginning and middle of test). This already is an indicator that the defected cell/s follow/s already a different degradation trend. As mentioned, at the end of test, this phenomenon become clear, with deviation between the maximum and minimum capacity for Pack N of 0.374 Ah. This deviation is reduced to about 0.111 Ah if the two outliers are not considered, which is still higher than the deviation shown for the Pack A (0.088 Ah). Eventually, looking at the temperature distributions shown in Fig. 9b, a temperature deviation of 1.42 °C between the maximum and minimum temperature is measured. At the beginning of test, maximum and minimum cell temperature are 25.17 °C and 23.75 °C respectively. During degradation, no remarkable increasing temperature trend can be noted on the contrary to Pack A: at the end of the test, a temperature deviation of 1.5 °C between the maximum (25.39 °C) and minimum temperature (23.89 °C) is measured.

3.2.6. Charge throughput

A further indication displaying the different aging between the two packs can be obtained by looking at the total Ah-throughput of each cell as a proportion of the total pack. The corresponding results are depicted in Fig. 10. The total pack capacity is taken as reference (equal to 1) and is scaled to the single cell capacity by dividing it by the number of cells in parallel. It is indicated by a dashed line in the plot. Accordingly, the total Ah-throughput of each cell during the entire test duration is normalized with respect to the total pack value. As it can be noted, for both pack the hottest cell (number 13 in the center) has the highest Ah-throughput. Moreover, the Ah-throughput for the Pack N is more uniformly distributed (18 cells above the average pack throughput, with a standard deviation of 0.0125 at the end-of-test not considering maximum and minimum values) than for the Pack A (12 cells above the average pack throughput, with a standard deviation of 0.013 at the end-of-test not considering maximum and minimum values), which give an indication of the uniform cell usage. Eventually, it become visible from the plot for the Pack N that not only the cells 22 and 7 contribute less to pack performance throughout its lifetime, but also cell 3 seems to show a stronger degradation behavior (i.e., smaller total Ah-throughput) with respect to the rest of the pack. These three cells will be focus of the second part of the paper and of the planed post-mortem analysis.

3.3. Discussion: technical and economic impact of immersion cooling system on battery pack design

In this section, a technical discussion regarding the possibility of employing the presented immersion cooling concept in a real application is presented. The aim is to transparently identify possible positive and negative aspects of using such cooling system in the automotive sector, analyzing most important key figures, such as system reliability and lifetime, safety, performance, and cost.

3.3.1. Reliability and lifetime

When designing a battery pack for a defined application, one of the key points is surely related to the system reliability, which is reflected directly in the corresponding lifetime. In this specific case, this is

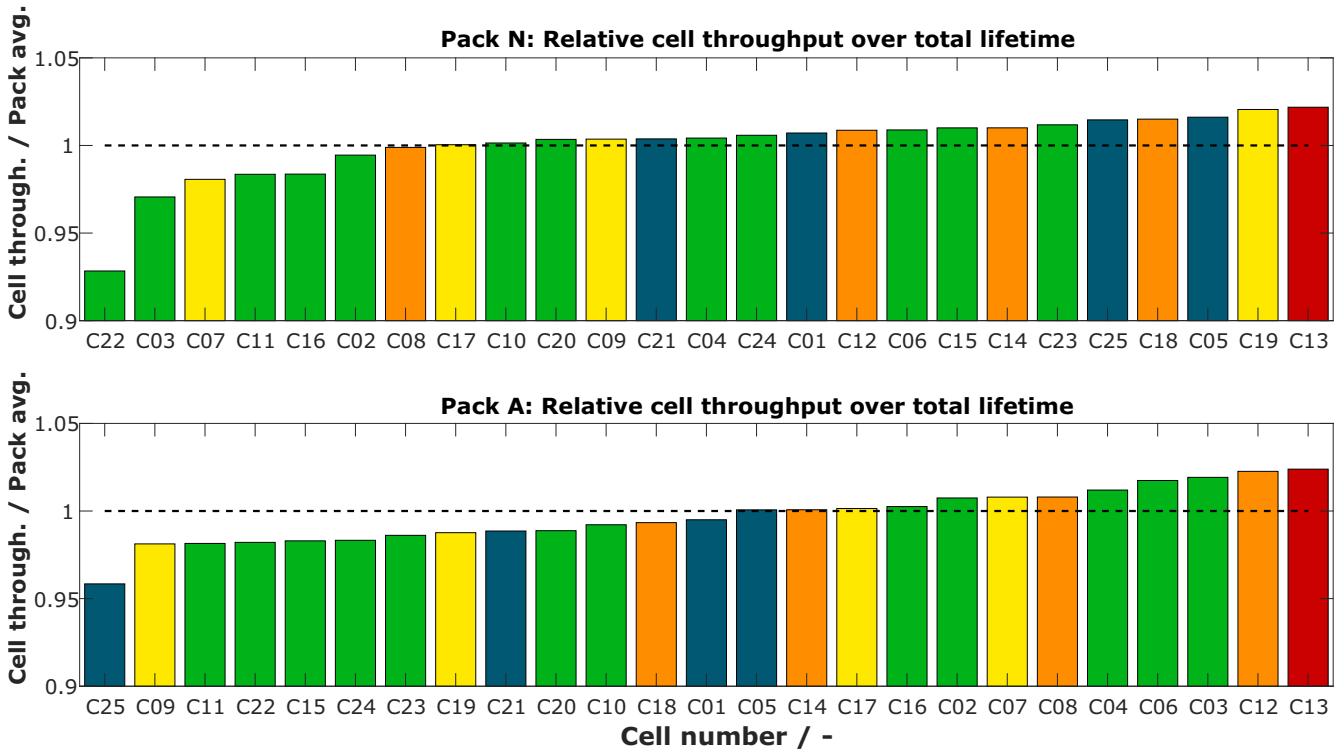

Fig. 10. Total charge throughput of all single cells until end-of-life criteria is reached. The Throughput of each cell is measured in respect of the average cell throughput (Throughput of Pack/25). The colors are chosen from the cells abilities to dissipate heat (refers to Fig. 1 and Table 1).

equivalent to the question: *is it worth to accept uneven temperature distribution among the cells to obtain higher battery pack capacity at cost of expected reduced lifetime?* The question has evidently not a single answer and shall be answered analyzing it by different perspectives. First, the most important point to address is whether for the application it is more important the absolute energy the pack can deliver in a specified condition or the lifetime. In case the pack, even accepting inhomogeneous temperature distribution among cells, can satisfy lifetime requirement, then the corresponding increase of performance (e.g., additional given range) becomes a crucial factor for the product, as the application lifetime is smaller than the generated pack lifetime. However, inhomogeneous temperature distribution generates cell with different aging states within the pack, which makes a second-life usage hardly possible or at least questionable. Second important point is the ambient temperature. In the presented case the air pack is cycled under ambient temperature of 23 °C, in reality, in many countries the ambient temperature can rise easily above 30 °C: in this case the cell temperature might reach accepted limits, inhibiting pack usage. For those cases a bigger battery pack is then needed, which generates smaller current rates at the same expected pack performance. Considering the experimental results, due to setup reasons, the two packs were cycled under the same ambient temperature, which generates for Pack N an average cell temperature of approx. 25 °C, and for Pack A a cell temperature between 30 °C and 45 °C. A fair comparison is evidently to change ambient temperature during cycling so that Pack N is operated at approx. 35 °C ambient temperature. This makes it difficult to a draw clear conclusion for the specific case regarding exclusively the benefit of homogeneous vs. inhomogeneous temperature distribution.

The last important point to be answered in this context is to quantify the increase of pack lifetime due to the usage of a mean which can guarantee homogeneous temperature distribution. As it can be observed in Fig. 6, the increase in pack capacity is approx. 2.4 %, 2.8 % and 3.3 % after 200, 400 and 600 EFC respectively between the Pack N and Pack A. A quantification and comparison of the final EOL is in this case questionable, due to the effect described in Section 3.2 and visible in Fig. 6: this is noticeable after approx. 600 EFC, with a change of pendency of the capacity fade curve only for the Pack N. The reason for this phenomenon will be analyzed in the second part of this paper. However, if this effect is hypothetically considered as due to some defected cells, then by means of extrapolating the capacity curve for the Pack N after 600 EFC, some conclusion can be drawn. This is shown in Fig. 11.

While Pack A shows a capacity of circa 77 % with 1058 EFC, the Pack N reaches the same capacity at around 1332 EFC, with a significant increase of lifetime of around 26 % with respect to the lifetime of Pack A. These results give quantitative hints to the effect of homogeneous temperature distribution. Eventually, it can be noted that the tested cells did not reach the critical region which lithium-ion cells usually experiences during degradation, i.e., the sudden abrupt of capacity due to a change of aging mechanism (normally recognized in the literature as lithium plating or loss of active material [52,53]).

3.3.2. Safety and maintenance

The use of a liquid coolant, which is in direct contact with the single cell surface has both merits and drawbacks when applied to a full system. First of all, checking the intrinsic property materials [47], the employed Novec™ 7200 fluid has a heat capacity of 1.220 $\frac{kJ}{kg \bullet K}$, which is slightly higher compared to that of air (1.005 $\frac{kJ}{kg \bullet K}$), and consequently has a higher heat dissipation capability. This is even more evident by analyzing volumetric heat capacity, where Novec™ 7200 fluid shows a heat capacity of 1969 $\frac{kJ}{m^3 \bullet K}$ against the one of the air of 1.2 $\frac{kJ}{m^3 \bullet K}$, a factor 1000 higher. Moreover, the employed material is non-flammable and low-toxic, and in a temperature range between −138 °C (freezing point) and 76 °C (boiling point) the fluid is highly chemically and thermally stable. Furthermore, the material is compatible with a number of metals and hard polymers, which is particularly relevant for a liquid immersion system presented, since the fluid is in direct contact with the battery cells. As outlined by Wang et al. [54], the case of currently commercially available 18650 consists of nickel plated cold-rolled steel. To ensure the compatibility of the Novec™ fluid with the battery shell material, long-

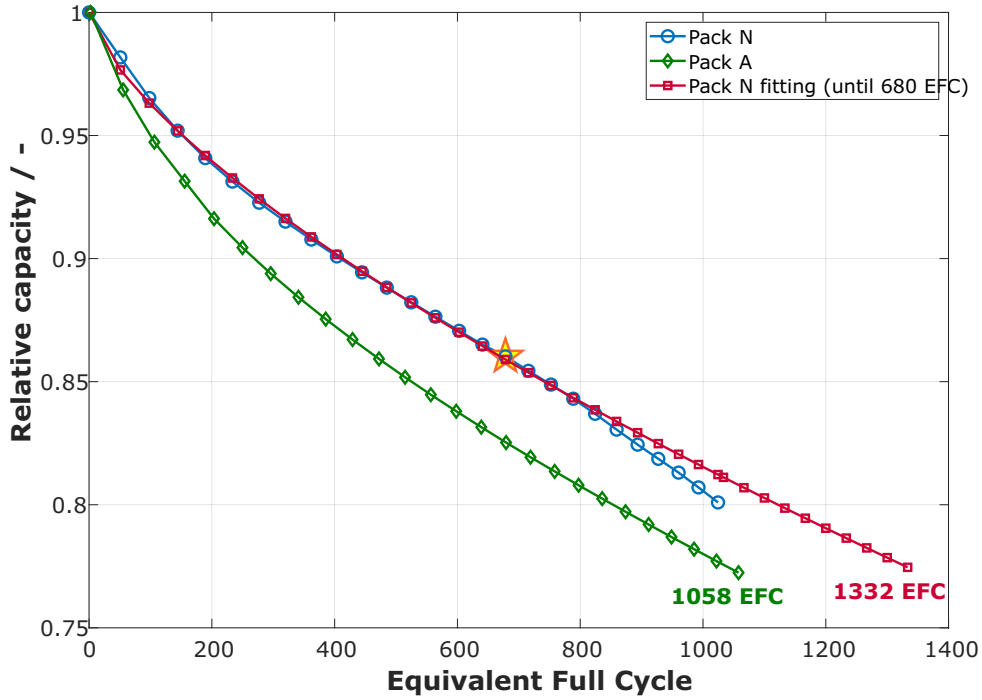

Fig. 11. Comparison of battery pack lifetime at EOL by extrapolation of lifetime for Pack N starting from approx. 680 EFC.

term exposure compatibility tests need to be performed. Due to its extremely low surface tension $(\sigma\text{Novec} = 13.6\ \frac{mN}{m} \approx \frac{1}{5}\ \sigma\text{water})$ the Novec™ fluid can easily spread out throughout the battery pack, thus allowing to reduce space among the cells [47,55]. This is also supported by the electrically insulating properties of this fluid. In summary, the chosen liquid guarantees in many points a better performance than air. However, when going to battery pack level many issues arise. The usage of a liquid generates the need of having a completely tight pack, which is not an easy task within the application, especially in case of accident and subsequent deformation in automotive applications. Therefore, leakage is always a huge problem in normal or extraordinary conditions. Moreover, when in contact with moisture or air, the Novec™ 7200 liquid decomposes and lead to gas generation. In this case, according to manufacturer, the corresponding gases are slightly toxic, but the Novec™ is not classified as hazardous material. Therefore, it is very likely that in real world applications the coolant must be replaced frequently, which leads to higher maintenance effort and costs as compared to air-cooled systems. To this, also the complexity of the system which circulates a fluid is evidently added, which is traduced in additional pumps, sensors and pipes which need to be maintained and substituted. Eventually, it is still to be clarified whether the Novec™ (or similar fluids) can penetrate inside lithium-ion cells which are not completely sealed. In this case, additional components might surely pollute the electrolyte, generating a reduction of battery lifetime.

3.3.3. Performance and cost

To generate a possible quantitative comparison of the performance of cooling solutions in application, a case study is presented. The target is to give the reader the necesseray means for comparing the presented solution without completely designing and sizing the chosen application. According to this, therefore, variations of single additional components energy consumption which shall be replaced is not considered in the calculation. The battery pack of a Nissan LEAF 2nd generation is considered as the reference system, as it is one of the few known and common applications in the market equipped with air-cooling system (the cells are cooled due to heat radiation into the overall battery pack) [56,57]. The 40 kWh battery pack of the LEAF is composed of 24 modules containing 8 cells each (192 lithium-ion pouch cells). Some of the most important pack figures are reported in Table 5.

Table 5
Most important figures for the battery pack of the Nissan LEAF 2nd generation [56,57].

Energy [kWh]	40
Range [km]	322
Number of modules	24
Cell per module	8
Weight [kg]	303
Volume [dm^3]	485.19

Based on this reference configuration, a similar pack with the 18650 cells tested within this work is roughly designed. As mentioned before, although a direct comparison between the LEAFs battery pack and the battery pack investigated in this work is hardly possible, as the latter contains several additional components, such as the battery management system, passive electrical components and battery housing, the aim is to point out the main differences regarding performance and costs. To reach the same energy of the Nisan LEAFs battery pack, 3900 cells of the type 18650 investigated in this paper are needed. Therefore, the 18650-pack will be characterized by a total cell weight and volume of approx. 181.74 kg and 67 dm^3 respectively, against the 175.5 kg and 85.5 dm^3 of the NISSAN-pack. Considering maintaining the same pack volume, this generates a volume difference between the NISSAN-pack and total 18650 cell volume of 418.18 dm^3. This volume can be used partially to be filled with the Novec™ coolant. For the Pack N presented in this paper, a total amount of 0.2465 dm^3 is employed, which results in approx. 0.00986 dm^3 per cell. Keeping the same proportion for the 18650-pack comparison, will surely not give the optimum solution, as in this work the content of Novec™ per cell was not optimized, but still yields an acceptable indication of performance trend. Therefore, for the 18650-pack, a total of 38.454 dm^3 of Novec™ coolant is needed. The Novec™ coolant is characterized by a density which changes with temperature, i.e., 1.61 kg/dm^3 at 25 °C and 1.59 kg/dm^3 at 35 °C. This results in additional 62 kg and 61.2 kg at 25 °C and 35 °C respectively. As the difference is negligible, considering an ambient temperature of 25 °C, and considering also additional weights of components for

Novec™ circulation within the pack between 20 and 40 kg, this results in a total 18650-pack specific energy of 102.25 Wh/kg and 97.28 Wh/kg respectively. Considering that the NISSAN-pack is characterized by a specific energy of 132.01 Wh/kg, in respect to it this means a reduction of 22.5 % and 26.3 % respectively.

The analysis of the costs is evidently influenced by many factors and cannot be tackled in a simplistic manner. However, to give an indication referred to the exemplary case presented, considering a price of Novec™ between 50 and 200 €/dm^3, this generates an additional price on the battery pack between approx. 1923 € and 7690 €, without considering the additional components for managing coolant circulation and tempering.

4. Conclusion

In the first of a series of two paper, an experimental degradation analysis of 18650 cylindrical cell battery pack with immersion liquid cooling system is presented. The focus of this paper is the aging analysis at pack level, while the second work will focus on the deep analysis of the degradation mechanisms at cell level. For the first time, the work presents a comprehensive experimental study on a compact immersion cooling system for cylindrical battery cell packs based on the 3M™ Novec™ 7200 cooling fluid. Two identical battery packs composed of 25 cylindrical 18650-type cells were cycled until EOL with air cooling and active immersed cooling thermal management strategies. This allows to analyze and quantify the degradation behavior on battery pack level in homogeneous and non-homogeneous temperature conditions. Main findings of the work can be summarized in the following points:

- By analyzing the obtained results on pack level, as expected the pack cycled under immersed cooling (Pack N) can maintain the cell temperature distribution rather uniformly, with a deviation between maximum and minim cell temperature of approx. 1.4–1.5 °C. On the other hand, for the pack cycled with air cooling (Pack A), a deviation between maximum and minimum cell temperature of approx. 13–15 °C was measured. This in turn generates a faster degradation of Pack A with respect to Pack N: at 600 EFC, the pack relative capacity for Pack A is already 3.3 % smaller than the capacity of Pack N.
- Unexpectedly, during the experiment, for some of the cells for the Pack N, the cell capacity fade trend started to deviate with respect to the majority, generating a knee in the total capacity fade curve, which was not visible for the Pack A. The reason for this might be due to multiple causes, which go from defected cells to possible intrusion of coolant within the cell can. The phenomenon will be investigated deeply in the second part of this paper where the identified cells once disassembled will be again tested and possibly undergo a post-mortem analysis. Nevertheless, when extrapolating battery pack lifetime, for a relative pack capacity of approx. 75 %, Pack N can be cycled with 275 EFC more than Pack A, demonstrating the merits and benefits of keeping temperature distribution homogeneous.
- A short technical application-oriented analysis is presented in the last part of the work, with the scope of discussing possible challenges of employing immersed cooling systems regarding performance, safety, maintenance, lifetime, and costs. By comparing the NISSAN Leaf 2nd generation battery with an 18650-pack having the same energy and being equipped with an immersed cooling system, the new battery pack will be affected by a possible reduction in terms of specific energy up to approx. 25 %. To get a fast overview over the advantages and drawbacks of the different cooling systems investigated, in Table 6 the properties of the two systems discussed in this work are compared and evaluated. This gives hints on how challenging it might be to exploit this kind of solution on the application level, even though some of the benefits are evident.

Table 6
Qualitative comparison of the two analyzed cooling systems.

	Air cooling	Immersed Cooling
Heat Transport Efficiency		
Temperature Homogeneity		
Safety		
Design		
Mass		
Maintenance		
Cost		

Legend: Bad, Good, Excellent.

CRediT authorship contribution statement

Dominique Koster: Writing final draft-review & editing. **Andrea Marongiu**: Data analysis and visualization, Writing final draft-review & editing. **Darya Chahardahcherik**: Conceptualization, Test setup and execution, Data analysis and visualization, Writing & review. **Carl Felix Braun**: Conceptualization, Test setup and execution, Review. **Dominik Schulte**: Conceptualization, Work supervision, Review. **Egbert Figgemeier**: Conceptualization, Work supervision, Review.

Declaration of competing interest

The authors declare that they have no known competing financial interests or personal relationships that could have appeared to influence the work reported in this paper.

Data availability

The data that has been used is confidential.

Acknowledgment

This work was supported and financed by the company BatterieIngenieure GmbH. The responsibility for this publication lies with the authors. Additionally, we would like to thank Izaro Laresgoiti and Timo Rüwald for the fruitful discussion and document review.

Appendix A. Supplementary data

Supplementary data to this article can be found online at https://doi.org/10.1016/j.est.2023.106839.

References

[1] T. Kim, W. Song, D. Son, L.K. Ono, Y. Qi, Lithium-ion batteries: outlook on present, future, and hybridized technologies, J. Mater. Chem. A 7 (2019) 2942–2964, https://doi.org/10.1039/C8TA10513H.
[2] Y. Ding, Z.P. Cano, A. Yu, J. Lu, Z. Chen, Automotive li-ion batteries: current status and future perspectives, Electrochem. Energy Rev. 2 (1) (2019) 1–28, https://doi.org/10.1007/s41918-018-0022-z.
[3] A. Naha, S. Han, S. Agarwal, A. Guha, A. Khandelwal, P. Tagade, K.S. Hariharan, S. M. Kolake, J. Yoon, B. Oh, An incremental voltage difference based technique for online state of health estimation of li-ion batteries, Sci. Rep. 10 (1) (2020) 9526, https://doi.org/10.1038/s41598-020-66424-9.
[4] S. Ma, M. Jiang, P. Tao, C. Song, J. Wu, J. Wang, T. Deng, W. Shang, Temperature effect and thermal impact in lithium-ion batteries: a review, Prog. Nat. Sci.: Mater. Int. 28 (6) (2018) 653–666, https://doi.org/10.1016/j.pnsc.2018.11.002.
[5] D. Chen, J. Jiang, G.-H. Kim, C. Yang, A. Pesaran, Comparison of different cooling methods for lithium ion battery cells, Appl. Therm. Eng. 94 (2016) 846–854, https://doi.org/10.1016/j.applthermaleng.2015.10.015.
[6] N. Yang, X. Zhang, B. Shang, G. Li, Unbalanced discharging and aging due to temperature differences among the cells in a lithium-ion battery pack with parallel combination, J. Power Sources 306 (2016) 733–741, https://doi.org/10.1016/j.jpowsour.2015.12.079.
[7] F. Gao, Z. Tang, Kinetic behavior of LiFePO4/C cathode material for lithium-ion batteries, Electrochim. Acta 53 (15) (2008) 5071–5075, https://doi.org/10.1016/j.electacta.2007.10.069.
[8] S.S. Zhang, K. Xu, T.R. Jow, The low temperature performance of li-ion batteries, J. Power Sources 115 (1) (2003) 137–140, https://doi.org/10.1016/S0378-7753(02)00618-3.

[9] T. Waldmann, M. Wilka, M. Kasper, M. Fleischhammer, M. Wohlfahrt-Mehrens, Temperature dependent ageing mechanisms in Lithium-ion batteries – a post-mortem study, J. Power Sources 262 (2014) 129–135, https://doi.org/10.1016/j.jpowsour.2014.03.112.

[10] M. Xiao, Theoretical and experimental analysis of heat generations of a pouch type LiMn2O4/carbon high power li-polymer battery, J. Power Sources 241 (2013) 46–5510, https://doi.org/10.1016/j.jpowsour.2013.04.062.

[11] Q. Wang, B. Jiang, B. Li, Y. Yan, A critical review of thermal management models and solutions of lithium-ion batteries for the development of pure electric vehicles, Renew. Sust. Energ. Rev. 64 (2016) 106–128, https://doi.org/10.1016/j.rser.2016.05.033.

[12] T. Baumhöfer, M. Brühl, S. Rothgang, D.U. Sauer, Production caused variation in capacity aging trend and correlation to initial cell performance, J. Power Sources 247 (2014) 332–3387, https://doi.org/10.1016/j.jpowsour.2013.08.108.

[13] M.J. Brand, M.H. Hofmann, M. Steinhardt, S.F. Schuster, A. Jossen, Current distribution within parallel-connected battery cells, J. Power Sources 334 (2016) 202–212, https://doi.org/10.1016/j.jpowsour.2016.10.010.

[14] B. Wu, V. Yufit, M. Marinescu, G.J. Offer, R.F. Martinez-Botas, N.P. Brandon, Coupled thermal-electrochemical modelling of uneven heat generation in lithium-ion battery packs, J. Power Sources 243 (2013) 544–554, https://doi.org/10.1016/j.jpowsour.2013.05.16.

[15] S. Paul, C. Diegelmann, H. Kabza, W. Tillmetz, Analysis of ageing inhomogeneities in lithium-ion battery systems, J. Power Sources 239 (2013) 642–650, https://doi.org/10.1016/j.jpowsour.2013.01.068.

[16] D. Kang, P.-Y. Lee, K. Yoo, J. Kim, Internal thermal network model-based inner temperature distribution of high-power lithium-ion battery packs with different shapes for thermal management, J. Energy Storage 27 (2020), 101017, https://doi.org/10.1016/j.est.2019.101017.

[17] C. Pastor-Fernández, T. Bruen, W.D. Widanage, M.A. Gama-Valdez, J. Marco, A study of cell-to-cell interactions and degradation in parallel strings: implications for the battery management system, J. Power Sources 329 (2016) 574–585, https://doi.org/10.1016/j.jpowsour.2016.07.121.

[18] Y. Deng, C. Feng, J. E, H. Zhu, J. Chen, M. Wen, H. Yin, Effects of different coolants and cooling strategies on the cooling performance of the power lithium ion battery system: a review, Appl. Therm. Eng. 142 (2018) 10–29, https://doi.org/10.1016/j.applthermaleng.2018.06.043.

[19] W.A. Hermann, Liquid Cooling Manifold With Multi-function Thermal Interface, Tesla Inc, US, 2010. US Patent US8263250B2.

[20] J. Perry, Webinar: EV battery thermal management. https://www.qats.com/cms/tag/electric-vehicles/. (Accessed 1 May 2022).

[21] R. Gogoana, M.B. Pinson, M.Z. Bazant, S.E. Sarma, Internal resistance matching for parallel-connected lithium-ion cells and impacts on battery pack cycle life, J. Power Sources 252 (2014) 8–13, https://doi.org/10.1016/j.jpowsour.2013.11.101.

[22] T. Bruen, J. Marco, Modelling and experimental evaluation of parallel connected lithium ion cells for an electric vehicle battery system, J. Power Sources 310 (2016) 91–101, https://doi.org/10.1016/j.jpowsour.2016.01.001.

[23] K.-H. Chen, T. Han, B. Khalighi, P. Klaus, Air cooling concepts for Li-ion battery pack in cell level, in: ASME Heat Transfer Summer Conference, July 9-14, 2017. Bellevue, WA, USA.

[24] T. Yuksel, S. Litster, V. Viswanathan, J.J. Michalek, Plug-in hybrid electric vehicle LiFePO4 battery life implications of thermal management, driving conditions, and regional climate, J. Power Sources 338 (2017) 49–64, https://doi.org/10.1016/j.jpowsour.2016.10.104.

[25] Y. Fan, Y. Bao, C. Ling, Y. Chu, X. Tan, S. Yang, Experimental study on the thermal management performance of air cooling for high energy density cylindrical lithium-ion batteries, Appl. Therm. Eng. 155 (2019) 96–109, https://doi.org/10.1016/j.applthermaleng.2019.03.157.

[26] Y. Wang, P. Peng, W. Cao, T. Dong, Y. Zheng, B. Lei, Y. Shi, F. Jiang, Experimental study on a novel compact cooling system for cylindrical lithium-ion battery module, Appl. Therm. Eng. 180 (2020), 115772, https://doi.org/10.1016/j.applthermaleng.2020.115772.

[27] H. Behi, D. Karimi, M. Behi, J. Jaguemont, M. Ghanbarpour, M. Behnia, M. Berecibar, J. Van Mierlo, Thermal management analysis using heat pipe in the high current discharging of lithium-ion battery in electric vehicles, J. Energy Storage 32 (2020), 101893, https://doi.org/10.1016/j.est.2020.101893.

[28] L. Feng, S. Zhou, Y. Li, Y. Wang, Q. Zhao, C. Luo, G. Wang, K. Yan, Experimental investigation of thermal and strain management for lithium-ion battery pack in heat pipe cooling, J. Energy Storage 16 (2018) 84–92, https://doi.org/10.1016/j.est.2018.01.001.

[29] C. Huber, Phase Change Material in Battery Thermal Management Applications, Technische Universität München, 2017.

[30] M. Safdari, R. Ahmadi, S. Sadeghzadeh, Numerical investigation on PCM encapsulation shape used in the passive-active battery thermal management, Energy 193 (2020), 116840, https://doi.org/10.1016/j.energy.2019.116840.

[31] Y. Wei, M. Agelin-Chaab, Development and experimental analysis of a hybrid cooling concept for electric vehicle battery packs, J. Energy Storage 25 (2019), 100906, https://doi.org/10.1016/j.est.2019.100906.

[32] Immersion cooling – potential alternative to traditional battery cooling. https://www.futurebridge.com/industry/perspectives-mobility/immersion-cooling-potential-alternative-to-traditional-battery-cooling/. (Accessed 1 May 2022).

[33] J. Edmondson, Immersion of electric vehicle batteries: the best way to keep cool?. https://www.idtechex.com/en/research-article/immersion-of-electric-vehicle-batteries-the-best-way-to-keep-cool/20169. (Accessed 1 May 2022). Dissertation RWTH Aachen, Germany.

[34] C. Roe, X. Feng, G. White, R. Li, H. Wang, X. Rui, C. Li, F. Zhang, V. Null, M. Parkes, Y. Patel, Y. Wang, H. Wang, M. Ouyang, G. Offer, B. Wu, Immersion cooling for lithium-ion batteries – a review, J. Power Sources 525 (2022), 231094, https://doi.org/10.1016/j.jpowsour.2022.231094.

[35] P. Nelson, D. Dees, K. Amine, G. Henriksen, Modeling thermal management of lithium-ion PNGV batteries, J. Power Sources 110 (2002) 349–356, https://doi.org/10.1016/S0378-7753(02)00197-0.

[36] G. Karimi, A.R. Dehghan, Thermal analysis of high-power lithium-ion battery packs using flow network approach, Int. J. Energy Res. 38 (2014) 1793–1811, https://doi.org/10.1002/er.3173.

[37] G.H. Kim, A. Pesaran, Battery thermal management system design modeling, in: 22nd International Battery, Hybrid and Fuel Cell Electric Vehicle Conference and Exhibition (EVS-22) Yokohama, Japan, October 23–28, 2006, https://doi.org/10.3390/wevj1010126.

[38] S. Park, D. Jung, Battery cell arrangement and heat transfer fluid effects on the parasitic power consumption and the cell temperature distribution in a hybrid electric vehicle, J. Power Sources 227 (2013) 191–198, https://doi.org/10.1016/j.jpowsour.2012.11.039.

[39] S.M.Hosseini Moghaddam, Designing Battery Thermal Management Systems (BTMS) for Cylindrical Lithium-ion Battery Modules Using CFD, KTH School of Industrial Engineering and Management, 2019. Master of Science Thesis.

[40] R.W. van Gils, D. Danilov, P.H.L. Notten, M.F.M. Speetjens, H. Nijmeijer, Battery thermal management by boiling heat-transfer, Energy Convers. Manag. 79 (2014) 9–17, https://doi.org/10.1016/j.enconman.2013.12.006.

[41] H. Hirano, T. Tajima, T. Hasegawa, T. Sekiguchi, M. Uchino, Boiling liquid battery cooling for electric vehicle, in: IEEE Conference and Expo Transportation Electrification Asia-Pacific (ITEC Asia-Pacific), Beijing, China, November 2014, https://doi.org/10.1109/ITEC-AP.2014.6940931.

[42] H. Zhou, C. Dai, Y. Liu, X. Fu, Y. Du, Experimental investigation of battery thermal management and safety with heat pipe and immersion phase change liquid, J. Power Sources 473 (2020), 228545, https://doi.org/10.1016/j.jpowsour.2020.228545.

[43] The primary challenge in electric motors is cooling, not lubrication. https://www.fuelsandlubes.com/fli-article/primary-challenge-electric-motors-cooling-lubrication/. (Accessed 1 May 2022).

[44] Excellent thermal control: immersion-cooling technology. https://www.xingmobility.com/technology. (Accessed 1 May 2022).

[45] High performance dielectric heat transfer fluids. https://www.solvay.com/en/brands/galden-pfpe. (Accessed 1 May 2022).

[46] Dielectric immersion cooling. https://www.batterydesign.net/dielectric-immersion-cooling/. (Accessed 22 December 2022).

[47] NOVEC product description. https://www.3mdeutschland.de/3M/de_DE/p/d/b40045142/. (Accessed 1 April 2022).

[48] Cell datasheet. https://cdn.shopify.com/s/files/1/0481/9678/0183/files/sony_vtc6_data_sheet.pdf?v=1605015770. (Accessed 10 April 2021).

[49] NOVEC datasheet. https://multimedia.3m.com/mws/media/338713O/3m-novec-7300-engineered-fluid.pdf. (Accessed 10 April 2021).

[50] D. Kim, K. Koo, J.J. Jeong, T. Goh, S.W. Kim, Second-order discrete-time sliding mode observer for state of charge determination based on a dynamic resistance li-ion battery model, Energies 6 (2013) 5538–5551, https://doi.org/10.3390/en6105538.

[51] D. Wang, Y. Bao, J. Shi, Online lithium-ion battery internal resistance measurement application in state-of-charge estimation using the extended Kalman filter, Energies 10 (2017) 1284–1294, https://doi.org/10.3390/en10091284.

[52] S.F. Schuster, T. Bach, E. Fleder, J. Müller, M. Brand, G. Sextl, A. Jossen, Nonlinear aging characteristics of lithium-ion cells under different operational conditions, J. Energy Storage 1 (2015) 44–53, https://doi.org/10.1016/j.est.2015.05.003.

[53] A. Marongiu, Performance and Aging Diagnostic on Lithium Iron Phosphate Batteries for Electric Vehicles and Vehicle-to-Grid Strategies, 2017, https://doi.org/10.18154/RWTH-2017-09944. Dissertation RWTH Aachen, Germany.

[54] L. Wang, S. Yin, Z. Yu, Y. Wang, T.X. Yu, J. Zhao, Z. Xie, Y. Li, J. Xu, Unlocking the significant role of shell material for lithium-ion battery safety, Mater. Des. 160 (2018) 601–610, https://doi.org/10.1016/j.matdes.2018.10.002.

[55] http://hyperphysics.phy-astr.gsu.edu/. (Accessed 1 April 2022).

[56] Nissan Leaf battery pack specifications. https://www.nissan-global.com/EN/TECHNOLOGY/OVERVIEW/li_ion_ev.html. (Accessed 1 April 2022).

[57] J. Nisewanger, Does the new 62 kWh LEAF battery have “an additional fan” for cooling?. https://electricrevs.com/2019/01/31/does-the-new-62-kwh-leaf-battery-have-an-additional-fan-for-cooling/. (Accessed 1 April 2022).